RSC Advances

ROYAL SOCIETY OF CHEMISTRY

www.rsc.org/advances

.

Structural, dielectric and magnetic investigations on Al^{3+} substituted Zn-ferrospinels

Naveen Kumari[1], Vinod Kumar[1], S. K. Singh[1]*

[1]Physics Department, DCR University of Science and Technology, Murthal -131039

naveenmalik6@yahoo.co.in

Abstract

A series of $ZnAl_xFe_{2-x}O_4$ ($0.1 \leq x \leq 0.5$) ferrospinels has been prepared by chemical co-precipitation method to understand the effect of Al^{3+} substitution on structural, dielectric and magnetic response of $ZnFe_2O_4$ nanoparticles. X-ray diffraction (XRD) and transmission electron microscopy (TEM) images confirmed the nano size formation of particles. The lattice parameter (a), X-ray density (ρ_x) and bulk density (ρ_m) were found to decrease with increasing inclusion of Al^{3+} ions. AC conductivity (σ_{ac}) measurements as a function of temperature show that the samples behave like semiconductors. Decrease in the hopping conduction between $Fe^{2+} \leftrightarrow Fe^{3+}$ ions at octahedral site is observed with increasing inclusion of Al^{3+} ions. The Nyquist plots of the prepared materials reveal the inherent phenomenon involved in conduction mechanism of Al^{3+} substituted $ZnFe_2O_4$ ferrites. The magnetization studies revealed that magnetic moment (η_B) showed decreasing trend with increase in substitution of Al^{3+}, its value decreases from 0.56 (for x=0.1) to 0.34 (for x=0.5). The M_s values decrease from 13.29 emu/gm for x=0.1 to 8.42 emu/gm for x=0.5. D_M (magnetic particle size) was found to be less than the particle size calculated from TEM micrographs due to presence of magnetically dead layer on the surface of particle. Squareness (S) values infer that particles interact by magnetostatic interactions. The M-H loop of

.

all the samples is narrow with low value of coercivity and retentivity; indicates the superparamagnetic nature of prepared nanoparticles.

Keywords: Ferrospinels, dielectric, nanosized, super-paramagnetic.

1. Introduction

Ferrospinels have attracted considerable attention due to their technological importance in different applications such as high frequency devices, biomedicine, catalysis, sensors, microwave absorbers, magnetic drug delivery and magnetic refrigerators [1, 2]. Spinel ferrites with general formula AB_2O_4 are widely used in many electronic and magnetic devices because of their high magnetic permeability and low magnetic loss [3]. Moreover, advanced applications often require materials with magnetic properties that can be deliberately tuned by external control parameters [4, 5]. The wide range of applications for ferrites is attributed to their resistivity, low eddy current losses, high Curie temperature, magnetocrystalline anisotropy, reasonable cost and excellent chemical stability [6]. In nanocrystalline phase magnetic, structural and electrical properties of ferrites change drastically in comparison to their bulk counterpart. This change in properties is also strongly dependent on preparation techniques, preparation conditions, site chosen for substitution and composition. Various methods (ceramic, sol-gel, co-precipitation, hydrothermal, auto-combustion [7-9], etc.) have been reported to generate nanosize materials. The ceramic method involves certain disadvantages including particle size inhomogeneity, high sintering temperatures, impurity introduced during grinding process [10]. Although chemical methods like co-precipitation and sol-gel are not economic for large scale production [11]. In the last decade, co-precipitation method has been extensively used for ferrites synthesis with metal nitrates or metal chlorides as cation sources, ammonia as precipitating agent and oleic acid as a surfactant to protect particles from atmospheric oxygen. The co-precipitation method produces

.

powders of homogeneous chemical composition, fine particle size, high yield, low preparation temperature and high chemical stability. It has been demonstrated by several experimental results that the A-site Zn^{2+} ions substitution is an effective method for tuning the physical properties of Fe_3O_4 [5]. Substitution of Fe^{3+} by Al^{3+} on B-site in ferrite nanoparticles modifies the structural, electrical and magnetic properties of ferrites [12]. The Al^{3+} substituted ferrites find a wide range of practical applications where minimum electrical and magnetic losses are required [13]. Several reports are available on Al^{3+} substituted Li ferrites [14], Al^{3+}substituted Ni-Zn ferrites [15] and Al^{3+} substituted Mg-Mn-Ni ferrites [12] etc. where various structural, dielectric and magnetic properties have been studied. However detailed reports are not available for Al^{3+} substituted $ZnFe_2O_4$ ferrite nanoparticles prepared via chemical co-precipitation method. In the present paper we have studied the effect of Al^{3+} substitution on various structural, dielectric and magnetic parameters at different frequencies and temperatures using XRD, Impedance analyzer and Vibrating sample magnetometer respectively. Evaluation of dielectric and magnetic parameters i.e. low loss, high resistivity and superparamagnetic nature of particles provides the information regarding the usefulness of materials in various practical applications where minimum core losses are required. Porosity of materials was found to be >70% making these materials useful for sensing applications.

2. Experimental

2.1 Materials & Sample preparation

A series of $ZnAl_xFe_{2-x}O_4$ (x = 0.1, 0.2, 0.3, 0.4 and 0.5) samples was prepared by chemical co-precipitation method. The materials required for synthesis viz. $ZnCl_2$, Al $(NO_3)_3.9H_2O$ and $Fe(NO_3)_3.9H_2O$ were procured from E-Merck, Germany and were used without further purification. Metal salts taken in required stoichiometric ratio were then dissolved in a required

.

amount of double distilled water and their homogeneous solutions were prepared using magnetic stirring. Oleic acid was added to avoid agglomeration of particles and to protect particles from atmospheric oxidation. Analytical grade ammonia (NH_3) solution was added drop by drop under constant stirring so as the pH of the solution attains value equal to 8 at which the precipitation of ferrites takes place. Required solution was then repeatedly washed with de-ionized water to remove unwanted salt residues and finally dried at 100^{o}C to remove remaining water contents [16]. Dried samples were then powdered using pestle and mortar for XRD, TEM and VSM analysis. The powdered samples were then pressed using hydraulic press under equal pressure conditions in the form of pallet of diameter 13mm and were used for dielectric analysis.

2.2 Characterization techniques

X-ray diffraction study of powdered samples annealed at 523K was carried out with a Panalytical X'Pert PRO X-ray diffractometer with CuK_α radiation (λ=1.5406Å) in the 2θ range of 20°-70° and with a scan rate of 2°/minute. Transmission electron microscopy studies were carried out from high resolution transmission electron microscopy analysis (HRTEM, Technai G2 200kV). Dielectric measurements were carried out using a HIOKI IM 3570 impedance analyzer in frequency range 1kHz to 5MHz and temperature range 300K to 523K. The M-H loops were recorded at room temperature with maximum applied field up to 15kOe.

3. Results and discussion

3.1 Structural Analysis

Fig. 1(a) shows the X-ray diffraction pattern of developed $ZnAl_xFe_{2-x}O_4$ (x = 0.1, 0.2, 0.3, 0.4 and 0.5) nanostructured particles. The XRD data reveals that all the composition exhibit single phase of prepared ferrites having space group Fd3m. Presence of diffraction planes (220), (311), (422),

.

(611) and (440) in the diffraction pattern confirms the formation of cubic spinel ferrite structure. In all the observed diffraction peaks a slight shift towards higher angle is being observed, indicating a little decrease in the unit cell of samples with increasing Al^{3+} content which shows that Al^{3+} ions have been incorporated into the spinel structure [17, 18]. The average crystalline size (*D*) (Table 1) of the particles was estimated using well known Debye-Scherrer formula [19].

$$D = \frac{k\lambda}{\beta \cos\theta} \quad \ldots(1)$$

Here λ is the wavelength of Cu-k_α radiation (λ=1.5406Å), β is FWHM in radians.

Present investigation shows that crystallite size of samples is in nanoscale range and decreases continuously with increasing inclusion of Al^{3+} ions concentration [20].

Lattice constant (a) has been calculated by d-spacing using the relation:

$$a = \frac{d}{\sqrt{h^2+k^2+l^2}} \quad \ldots (2)$$

Where (h, k, l) are the miller indices. As shown in Table 1 lattice constant was found to decrease linearly with increasing substitution of Fe^{3+} by Al^{3+} obeying Vegard's law [20]. The decrease in lattice constant is attributed to the fact that the ionic radii of Al^{3+} ~(0.54Å) ions is smaller than that of Fe^{3+} ~(0.67Å) ions.

X-ray density (ρ_x), apparent density (ρ_m) and porosity (*P*) as shown in (Table 1) has been calculated using following standard relations shown in eq. 3, eq. 4 and eq. 5 respectively.

$$\rho_x = \frac{8\,X\,M}{NV} \quad \ldots (3)$$

M is molecular weight of sample, N is Avogadro's number

$$\rho_m = \frac{m}{\pi r^2 h} \quad \ldots (4)$$

.

Where m is mass, r is radius, h is height of sample for cylindrical pallets of the samples.

$$P = 1 - \frac{\rho_m}{\rho_x} \quad \ldots (5)$$

Both X-ray density and apparent density show decreasing trend with increasing content of Al^{3+} ions as density and atomic weight of Aluminium atoms (2.702 gm/cc and 26.98154 gm) is less than that of iron atoms (7.86 gm/cc and 55.845 gm) [21]. The X-ray density is higher than apparent density. This may be due to the existence of pores in the samples, which depend upon sintering conditions (apparent density calculations were executed using pellets made by applying 25 N/m^2 pressure for 5 minutes to the powdered samples. Pellets so formed were sintered at 200^0C for 1 hour). In addition, the porosity shows increasing trend with increasing Al^{3+} ion content, which is due to lower density of Al^{3+} ions, revealing that aluminium enhances the disorder of spinel ferrite system. Relatively large porosity values for nanosize samples and low temperature sintered ferrites are commonly observed [22].

For cubic spinel structures X-Ray parameters viz. A-site radii (r_A) , B-site radii (r_B) [23], tetrahedral bond length (d_{AL}), octahedral bond length (d_{BL}) [24], jump length of A-site (L_A) and jump length of B-site (L_B) [25] as shown in (Table 1) were calculated using values of lattice constant (a) and oxygen positional parameter (u) from the equations (6) to (11).

$$r_A = (u - 0.25)a\sqrt{3} - R_0 \quad \ldots (6)$$

Here u =3/8 and R_0 is oxygen ion radius [26, 27]

$$r_B = (0.625 - u)a - R_0 \quad \ldots(7)$$

$$d_{AL} = (u - 0.25)a\sqrt{3} \quad \ldots(8)$$

.

$$d_{BL} = a\sqrt{\left(3u^2 - \frac{11}{4u} + \frac{43}{64}\right)} \quad \ldots(9)$$

$$L_A = \frac{a\sqrt{3}}{4} \quad \ldots(10)$$

$$L_B = \frac{a\sqrt{2}}{4} \quad \ldots(11)$$

It is observed that r_A, r_B, d_{AL} and d_{BL} decrease with increasing substitution of Fe^{3+} by Al^{3+} ions content which may be due to the increasing substitution of the smaller ionic radii Al^{3+} ~(0.54Å) ions at octahedral site (B-site) instead of Fe^{3+} ~(0.67Å) ions. The decreasing trend of L_A and L_B with increasing Al^{3+} content is due to decrease in distance between magnetic ions by the substitution of smaller Al^{3+} at octahedral site [28]. From Table 1, it is also observed that $L_A > L_B$ which indicates that the electron hopping between ions at A and B sites is less probable than that between B and B sites.

Fig. 1(b) shows the typical EDAX spectrum of the composition $ZnAl_{0.5}Fe_{1.5}O_4$. The spectrum marks the presence of Zn, Al, Fe and O which further confirms the formation of pure $ZnAl_{0.5}Fe_{1.5}O_4$. Fig. 2 shows the TEM micrographs of $ZnAl_xFe_{2-x}O_4$ (x = 0.1, 0.3, and 0.5) samples. It is observed from TEM images that the particles are little agglomerated. The agglomeration can be attributed to magnetic interaction arising among ferrite nanoparticles. The average particle sizes for x = 0.1, x = 0.3 and x = 0.5 samples are ~ 31nm, ~ 29nm and ~ 26nm respectively.

3.2 Temperature and frequency dependent dielectric properties

.

Various dielectric parameters i.e. the real (ε') and imaginary (ε'') parts of dielectric constant, dielectric loss tangent ($tan\delta$) and ac conductivity (σ_{ac}) were calculated using standard relations of eq. 12, eq. 13 and eq. 14 respectively.

$$\varepsilon' = \frac{Ct}{\varepsilon_0 A} \quad \ldots (12)$$

Where C is capacitance in farad (F), A is cross-sectional area of pallet in m^2, t is the thickness of the pallet in mm and ε_0 is constant of permittivity in free space

$$\varepsilon'' = \varepsilon' \tan\delta \quad \ldots (13)$$

$$\sigma_{ac} = 2\pi f \varepsilon' \varepsilon_0 \tan\delta \quad \ldots (14)$$

Where f is frequency of alternating applied field in Hz.

3.2.1 Real (ε′) and imaginary (ε″) part of dielectric constant

Fig.3 and Fig.4 show the variation of real and imaginary part of dielectric constant of nano $ZnAl_xFe_{2-x}O_4$ (x = 0.1, 0.2, 0.3, 0.4 and 0.5) ferrite samples with frequency from 1kHz to 5MHz at 523K. It can be observed that all the compositions exhibit dielectric dispersion where both real and imaginary part of dielectric constant decreases rapidly with frequency in low frequency region while it behaves almost frequency independent in high frequency region. This type of decrease can be explained on the basis of Koop's theory [29] in accordance with Maxwell-Wagner two layer model for in-homogeneous structure [30] as during the preparation of ferrites in poly-crystalline form the formation of highly conducting grains with thin layers of poorly conducting grain boundaries take place. Thus they behave as heterogeneous dielectric materials. According to Maxwell-Wagner model, structure of ferrite materials are supposed to be consisted of highly conducting phases (grains) in insulating matrix (poorly conducting grain boundaries)

.

[31, 32]. At lower frequencies grain boundaries are more effective and as frequency increases highly conducting grains come in action due to which dielectric constant decreases. Further analysis of variation of ε' and ε'' shows that both of these dielectric parameters have high value at lower frequency and its value becomes so small that it becomes frequency independent at higher frequencies which can be explained on the basis of space charge polarization [31] which is produced due to presence of high conducting phases (grains) in between thin poorly conducting grain boundaries. Electron exchange between $Fe^{2+} \leftrightarrow Fe^{3+}$ results in the local displacement of electrons in the direction of applied field that determines the polarization in ferrites. On the application of alternating electric field as the electrons reach the poorly conducting grain boundary they pile up there and cause space charge polarization due to which the dielectric constant is high at low frequencies and as frequency increases polarization decreases. According to classical polarization mechanism, as frequency increases mobility of electrons in between ferrous and ferric ions decreases because of which surface charge polarization contribution effect decreases and gets eliminated [32-34]. At sufficiently higher frequencies of external applied field electronic movements are not able to keep pace with rapidly changing ac field as charge carriers require finite time to change their orientation in response to the applied electric field [35]. It is because of the predominance of species like Fe^{2+} ions, oxygen vacancies, grain boundary defects, interfacial dislocation pile ups, voids, etc. [30, 36]. Also, the dielectric constant decreases with increasing substitution of Fe^{3+} ions by Al^{3+} ions because of decreasing availability of ferrous and ferric ions at octahedral site which are preferentially occupied by Al^{3+} ions.

Inset of Fig.3 and Fig.4 show the temperature dependence of ε' and ε'' at 10kHz, 100kHz and 1MHz for x=0.1. Analysis shows that there is increase in the value of ε' and ε'' with increase in

.

temperature. This increase an in dielectric constant could be because of increase in drift mobility of charge carriers as electron hoping between Fe^{2+} (Ferrous) and Fe^{3+} (Ferric) ions present at octahedral site is thermally enhanced with increasing temperature which causes local displacement in the direction of applied electric field which in turn enhance their contribution to the space charge polarization [37] .This leads to increase in the value of ε' and ε''. It is observed that, this increase is quite significant at lower frequencies and as frequency increases the increase in dielectric constant (ε′) becomes quite insignificant. It is known that polarization of ferrite materials, in general, is due to interfacial, dipolar, electronic and ionic polarization [38]. Dipolar and interfacial polarization are known to play dominant role at lower frequencies and both are temperature dependent [39]. At higher frequencies electronic and ionic polarization are main contributors and do not depend significantly upon temperature [38]. So an increase in the value of ε′ and ε″ with temperature at lower frequencies arises from the combined effect of dipolar and interfacial polarizations. At high frequencies the variation of ε' and ε'' with temperature is insignificant due the dominant effect of ionic and electronic polarization. Dielectric constant of these ferrites is sufficiently low which is probably due to low sintering temperature during preparation. Sintering at lower temperature results in reducing the possibility of ions to exist in different valance states and ultimately reduces the probability of electron hopping.

3.2.2 Dielectric loss ($\tan\delta$)

The variation of dielectric loss with frequency was studied at 523K and is depicted in Fig. 5. It is clear that dielectric loss shows normal dielectric behavior for all the samples. Again the dielectric loss decreases with increase in frequency at low frequencies and becomes almost frequency independent at higher frequencies. Conduction in ferrites is due to hopping between ions of same element at octahedral site. When the frequency of applied ac electric field is much

.

smaller than the hopping frequency of electrons between ferrous and ferric ions at octahedral site, electrons follow the field and loss is maximum. At higher frequencies electron exchange between Fe^{2+} and Fe^{3+} ions can't keep pace with applied ac electric field which causes a decrease in contribution of space charge polarization and we observe a decrease in dielectric loss. The high value of dielectric loss at low frequencies is due to high resistivity of grain boundaries which are more effective at lower frequencies. Due to high resistivity of grain boundaries more energy is required for electron exchange between ferrous (Fe^{2+}) and ferric (Fe^{3+}) ions, which corresponds to maximum energy loss. On the other hand with increase in frequency small energy is sufficient for electron exchange, which corresponds to less energy loss [40, 41]. It is also observed that tanδ of prepared nano particles depends upon the composition. It decreases with increasing inclusion of Al^{3+} ions. Inset of Fig.5 shows the temperature dependence of tanδ at 10kHz, 100kHz and 1MHz for x=0.1. It is observed that there is an increase in the values of tanδ with increase in temperature. It is also observed that, this increase is quite significant at lower frequencies and as frequency increases this increase in dielectric loss becomes quite insignificant which can be explained on the same basis as in the case of dielectric constant.

3.2.3 AC conductivity (σ_{ac})

Fig.6 shows the frequency dependence of ac conductivity (σ_{ac}) at 523K for all the prepared samples. Analysis shows that the total conductivity almost remains constant in lower frequency region, slowly increases in middle frequency region and shows dispersion for higher frequency region which is in accordance with eq 15.

$$\sigma_{tot} = \sigma_0(T) + \sigma(\omega, T) = \sigma_0(T) + B\omega^s \quad \ldots(15)$$

.

Where first part is dc conductivity and is due to band conduction which is frequency independent part [42] and second part is ac conductivity due to hopping mechanism among ions of same element which are present in more than one valance state. 'B' and 's' are constants which depend on both temperature and composition; s is a dimensionless quantity having values between 0 and 1, when s = 0 conduction is dc conduction, but for s ≤ 1, the conduction is ac conduction. 'B' has the dimensions of electrical conductivity. The conductivity of samples increases with increasing frequency which is universal dielectric behavior and can be explained on the basis of hopping model. In the low frequency region, grain boundaries are more effective with high resistance due to which we obtain constant plateau region (σ_{dc}). At higher frequencies, the increase in conductivity is due to increased hopping of charge carriers between Fe^{2+}/ Fe^{3+} ions at octahedral site and also due to grain effect [43]. With the increase in substitution of Fe^{3+} by Al^{3+} ions conductivity decreases due to its stable oxidation state of Al^{3+} ion which do not participate in conduction and also limits the conduction between Fe^{3+} and Fe^{2+} ions as Al^{3+} ion preferentially occupy octahedral site. Inset of Fig.6 represents the variation of σ_{ac} for x=0.1 with temperature at different frequencies i.e. 1kHz, 100kHz and 1MHz. It is observed that σ_{ac} increases with increase in temperature which may be due to increased hopping of charge carriers and increase in grain size as a result of which number of grain boundaries decreases with increasing temperature [44].

3.2.4 Impedance spectroscopy

Impedance measurements were carried out in the frequency range of 1kHz to 5MHz at 523K. The impedance spectroscopy helps us to distinguish the effect of grains and grain boundaries because both of them have different relaxation time. Impedance spectroscopy (Cole-Cole) is studied by plotting real part (Z') with imaginary (Z'') part of impedance. Fig.7 (a) shows impedance spectroscopy measurements for $ZnAl_xFe_{2-x}O_4$ (x = 0.1, 0.2, 0.3, 0.4 and 0.5) at 523K.

.

Analysis of plots shows that the diameter of semicircle increases with increasing Al^{3+}substitution which means impedance increases which supports the decrease in conductivity and increase in relaxation time. Variation of Cole-Cole plots also supports the variation in dielectric parameters and ac conductivity. After extrapolating the Cole-Cole plots what we observe is that all these semicircles merge and terminate at Z' (real) axis at higher frequency side, this indicates the presence of bulk resistance. Also, grain boundary resistance is there but it is very small as no second semicircle is obtained [45, 46]. The values of R_g (grain resistance), C_g (grain capacitance), τ_g (relaxation time) are calculated for $ZnAl_xFe_{2-x}O_4$ (x = 0.1, 0.2, 0.3, 0.4 and 0.5) and are reported in Table 2. C_g (grain capacitance) is calculated using frequency peaks of semicircle arcs at maximum $Z' = -Z''$.

$$C_g = \frac{1}{R_g \omega_g} \quad \ldots (16)$$

$$\tau_g = \frac{1}{\omega_g} = C_g R_g \quad \ldots (17)$$

Fig. 7(b) shows Cole-Cole plots of $ZnAl_xFe_{2-x}O_4$ (x = 0.1) sample at different temperatures i.e. 423K, 473K and 523K. Analysis shows that the diameter of semicircle decreases with increasing temperature which means impedance decreases that support the increase in conductivity and decrease in relaxation time. The values of R_g, C_g, τ_g calculated at different temperatures are reported in Table 3.

4. Magnetic Analysis

Fig. 8(a) shows the variation of the magnetization (M) as a function of applied magnetic field (H) for $ZnAl_xFe_{2-x}O_4$ (x=0.1, 0.2, 0.3, 0.4, 0.5) ferrite samples measured at room temperature. Variation in various magnetic parameters i.e. saturation magnetization (M_S), remanence

.

magnetization (M_r), coercivity (H_C), anisotropy constant (K), squareness (S) [represented as a measure of how square the loop is and is a dimensionless quantity between 0 and 1]and magnetic moment (η_B) as a function of substitution of Fe^{3+} by Al^{3+} ions is shown in Table 4. The M_S, M_r and H_c values gradually decreases with increasing inclusion of Al^{3+}. The M_s values decrease from 13.29 emu/gm for x=0.1 to 8.42 emu/gm for x=0.5. This may be due to the fact that Fe^{3+} ions (magnetic moment 5μB) are replaced by lesser magnetic Al^{3+} (magnetic moment 0μB) ions at the octahedral B-sites of ferrite sublattice [47]. It is observed that the magnetic moment decreases with Al^{3+} substitution which may also be due to substitution of lesser magnetic Al^{3+} ions which have strong site preference for octahedral B-site [48]. From the hysteresis loops S is derived to determine whether the intergrain exchange exists or not [49]. Stoner and Wohlfarth have reported S=0.5 for randomly oriented non-interacting particles, while S< 0.5, particles interact by magnetostatic interaction [50]. In this study, for all samples, S values are less than 0.5 indicating that particles interact by magnetostatic interactions. Upper limit of magnetic particle size (D_m) was calculated from M-H loop using the relation [51, 52]:

$$D_m = \sqrt[3]{\frac{18K_BT\chi_i}{\pi\rho(M_S)^2}} \quad \ldots (18)$$

where k_B is Boltzmann's constant, T is measurement temperature, χ_i is initial magnetic susceptibility ($\chi_i=(dM/dH)_{H\to0}$), ρ is density and M_s is saturation magnetization of sample. D_M was found to be less than the particle size calculated from TEM micrographs due to presence of magnetically dead layer on the surface of particle. As the surface layer of dimensions nearly half the unit cell dimensions do not contribute towards magnetization and thus magnetic particle size comes out to be less than the particle size calculated from electron microscopy data. Low values of retentivity and coercivity reveals that Al^{3+} substituted Zn-ferrite particles are

.

superparamagnetic in nature. Fig. 8(b) shows the typical hysteresis loop of the sample with composition $ZnAl_{0.1}Fe_{1.9}O_4$ annealed at two different temperatures (523 and 773K) along with those of as obtained sample. Similar type of behavior was observed for other compositions also. It is observed from Fig. 8(b) that M_s value increases with increase in annealing temperature possibly due to the fact that increase in annealing temperature results in an increase in particle size. Consequently, a decrease in the amount of super-paramagnetic particles occurs which allows an increase in overall magnetization [53, 54].

5. Conclusions

In the present study, single phase ferrospinels $ZnAl_xFe_{2-x}O_4$ (x = 0.1, 0.2, 0.3, 0.4 and 0.5) were successfully synthesized by chemical co-precipitation method. The structure and nano size of prepared samples were confirmed using XRD method and TEM images. Lattice parameter (a), X-Ray density (ρ_x), apparent density (ρ_m) has been found to decrease with Al^{3+} substitution which is explained on the basis of smaller ionic radii and density of Al^{3+} ion. However, increasing trend in porosity was attributed to the substitution of Fe^{3+} by Al^{3+} ions, thereby, making all samples porous. The dielectric parameters show normal dielectric behavior with frequency and temperature which is explained on the basis of Koop's theory in accordance with Maxwell –Wagner two layer model by taking surface charges into account. The dielectric properties i.e. real and imaginary part of dielectric constant (ε' & ε''), dielectric loss ($tan\delta$) and ac conductivity (σ_{ac}) decrease with Al^{3+} ion substitution. The area under the semicircle of cole-cole plots increases with increasing inclusion of Al^{3+}ions which also support the decrease in conductivity. It has been observed that as temperature increases, the area under the semicircle of Cole-Cole plots decreases, which represents the tendency of better conductivity of samples. Low value of dielectric loss ($tan\delta$) and high resistivity obtained in these ferrites is suitable for devices

.

where low eddy current losses are required in low as well as high frequency region. Saturation magnetization was found to be decreasing with increasing Al^{3+} substitution which was due to less magnetic moment of Al^{3+} ions as compared to the magnetic moment of Fe^{3+} ions. Values of coercivity and retentivity were found to be very small due to super-paramagnetic nature of particles. Squareness (*S)* values revealed that particles interact by magnetostatic interactions.

Acknowledgements

The authors are greatly thankful to UGC, New Delhi (India) for providing financial support under Major Research Project (F.No.39-500/2011 (SR)) at department of physics, DCR University of science and technology, Murthal, Haryana, India**.** Co-ordinator CIL, DCRUSTM is also acknowledged for providing the Impedance Analyzer facility. Sincere acknowledgement is expressed to Director SAIF (IIT Chennai) for providing VSM facility.

References

[1] S. Odenbach, Ferrofluids, Springer, Berlin Heidlberg, 2002.

[2] S. Adarsh, H. Hiroshi, A. Masanori, Synthesis and applications of magnetic nanoparticles for biorecognition and point of care medical diagnostics, Nanotechnology 21 (2010) 442001.

[3] L. Hao, Y. Zhao, Q. Jiao, P. Chen, Synthesis of zinc–nickel ferrite nanorods and their magnetic properties, RSC Adv. 4 (2014) 15650.

[4] D. Venkateshvaran, M. Althammer, A. Nielsen, S. Geprägs, M.S. Ramchandra Rao, S.T.B. goennenwein, M. Opel, R. Gross, Epitaxial $Zn_xFe_{3-x}O_4$ thin films: A spintronic material with tunable electrical and magnetic properties, Phys. Rev. B: Condens. Matter Mater. Phys., 74 (2009) 134405.

.

[5] Y.H. Cheng, L.Y. Li, W.H. Wang, H. Liu, S.W. Ren, X.Y. Cui, R.K. Zheng, Tunable electrical and magnetic properties of half-metallic $Zn_xFe_{3-x}O_4$ from first principles, Phys. Chem. Chem. Phys. 13 (2011) 21243.

[6] A.M. Wahba, N.A. Ali, M.M. Eltabey, Effect of Al-ion substitution on structural and magnetic properties of Co–Ni ferrites nanoparticles prepared via citrate precursor method, Mater. Chem. Phys. 146 (2014) 224

[7] Sagar E. Shirsath, R. H. Kadam, S. M. Patange, M. L. Mane, Ali Ghasemi, Akimitsu Morisako, Enhanced magnetic properties of Dy^{3+} substituted Ni-Cu-Zn ferrite nanoparticles, Appl. Phys. Lett. 100 (2012) 042407.

[8] Jian-Min Li, Xian-Lin Zeng, Zhu-An Xu, Partial cationic inversion-induced magnetic hardening of densely packed 23-nm-sized nanocrystallite-interacting nickel ferrite electrospun nanowires, Appl. Phys. Lett. 103 (2013) 232410.

[9] H.W. Wang, S.C. Kung, Crystallization of nanosized Ni–Zn ferrite powders prepared by hydrothermal method, J. Magn. Magn. Mater. 270 (2004) 230.

[10] A.R. Bueno, M.L. Gregori, M.C.S. Nobrega, Effect of Mn substitution on the microstructure and magnetic properties of $Ni_{0.50-x}Zn_{0.50-x}Mn_{2x}Fe_2O_4$ ferrite prepared by the citrate–nitrate precursor method, Mater. Chem. Phys. 105 (2007) 229.

[11] R.V. Mangalaraja, S. Ananthakmr, P. Manohara, F.D. Gnanama, M. Awano, Characterization of $Mn_{0.8}Zn_{0.2}Fe_2O_4$ synthesized by flash combustion technique, Mater. Sci. Eng. A 367 (2004) 301.

.

[12] S. Verma, J. Chand, M. Singh, Structural and electrical properties of Al^{3+} ions doped nanocrystalline $Mg_{0.2}Mn_{0.5}Ni_{0.3}Al_yFe_{2-y}O_4$ ferrites synthesized by citrate precursor method, J. Alloys Compd. 587 (2014) 763.

[13] M. Kisielewski, A. Maziewski, M. Tekielak, J. Ferre, S. Lemerle, V. Mathet, C. Choppert, Magnetic anisotropy and magnetization reversal processes in Pt/Co/Pt films, J. Magn. Magn. Mater. 260 (2003) 231.

[14] M. A. Dar, K. M. Batoo, V. Verma, W. A. Siddiqui, R. K. Kotnala, Synthesis and characterization of nano-sized pure and Al-doped lithium ferrite having high value of dielectric constant, J. Alloys Compds. 493 (2010) 553.

[15] M. Hasim, Alimuddin, S. Kumar, S. Ali, B. H. Koo, H. Chung, R. Kumar, Structural, magnetic and electrical properties of Al^{3+} substituted Ni–Zn ferrite nanoparticles, J. Alloys Compds. 511 (2012) 107.

[16] N. Kumari, V. Kumar, S.K. Singh, Synthesis, structural and dielectric properties of Cr^{3+} substituted Fe_3O_4 nano-particles, Ceram. Int. 40 (2014) 12199.

[17] J. A. Toledo, M. A. Valenzuela, P. Bosch, H. Armendariz, A. Montoya, N. Nava and A. Vazquez, Effect of AI^{3+} introduction into hydrothermally prepared $ZnFe_2O_4$, Appl. Catal. A 198 (2000) 235.

[18] N. Kumari, V. Kumar, S.K. Singh, Dielectric study of Al^{3+} transition metal doped Fe_3O_4 ferrite nanoparticles, Int. J. Modern Phys. B 28 (2014) 1450193.

[19] B. D. Cullity Elements of X-ray Diffraction, Addision-Wesely, Reading, MA, USA (1978).

.

[20] C.G. Whinfrey, D.W. Eckart, A. Tauber, Preparation and X-Ray Diffraction Data[1] for Some Rare Earth Stannates, J. Am. Chem. Soc. 82 (1960) 2695.

[21] M. A. Dar, K. M. Batoo, V. Verma, W. A. Siddiqui, R. K. Kotnala, Synthesis and characterization of nano-sized pure and Al-doped lithium ferrite having high value of dielectric constant, J. Alloys Compds. 493 (2010) 553.

[22] M. Hasim, Allimudin, S. Kumar, B.H. Koo, S.E. Shirsath, E.M. Mohammed, J. Shah, R.K. Kotnala, H.K. Choi, H. Chung, R. Kumar, Structural, electrical and magnetic properties of Co–Cu ferrite nanoparticles, J. Alloys Compds. 518 (2012) 11.

[23] J. Smit, H.P.J. Wijn, Ferrites-Physical Properties of Ferromagnetic Oxides in Relation to their Technical Applications, N.V. Philips Gloeilampenfabrienken, Eindhoven, 1959.

[24] M.A. Amer, ^{57}Fe Mössbauer, Infrared and X-Ray Studies of the System $Zn_{1-x}Cu_xCr_{0.8}Fe_{1.2}O_4$, Phys. Status Solidi A, 181 (2000) 539.

[25] A. Globus, H. Pascard, V. Cagan, Distance between Magnetic Ions and Fundamental Properties in Ferrites, J. Physique Coll, 38 (1977) 163.

[26] M.F. Al-Hilli, S. Li, K.S. Kassim, Microstructure, electrical properties and Hall coefficient of europium-doped Li–Ni ferrites, Mater. Sci. Eng. B, 158 (2009) 1.

[27] K.J. Standley, Oxide Magnetic Materials, 2nd edition, Oxford University Press, 1972, p.28.

[28] S. Verma, J. Chand, M. Singh, Structural and electrical properties of Al^{3+} ions doped nanocrystalline $Mg_{0.2}Mn_{0.5}Ni_{0.3}Al_yFe_{2-y}O_4$ferrites synthesized by citrate precursor method, J. Alloys Compds. 587 (2014) 763.

[29] C.G. Koops, On the dispersion of resistivity and dielectric constant of some semiconductors at audiofrequencies, Phys. Rev. 83 (1951) 121.

.

[30] K.W. Wagner, E.L. Heilman, The distribution of relaxation times in typical dielectrics, Ann. Phys. 40 (1993) 818.

[31] A. Rana, O.P. Thakur, V. Kumar, Effect of Gd^{3+} substitution on dielectric properties of nano cobalt ferrite, Mater. Lett. 65 (2011) 3191.

[32] S.M. Patange, S.E. Shirsath, K.S. Lohar, S.S. Jadhav, N. Kulkarni, K.M. Jadhav, Electrical and switching properties of $NiAl_xFe_{2-x}O_4$ ferrites synthesized by chemical method, Phys. B 406 (2011) 663.

[33] A.M.M. Farea, S. Kumar, K.M. Batoo, A. Yousef, C.G. Lee, Alimuddin, Structure and electrical properties of $Co_{0.5}Cd_xFe_{2.5-x}O_4$ ferrites, J. Alloys Compd. 464 (2008) 361.

[34] M. Tan, Y. Köseoğlu, F. Alan, E. Sentürk, Overlapping large polaron tunneling conductivity and giant dielectric constant in $Ni_{0.5}Zn_{0.5}Fe_{1.5}Cr_{0.5}O_4$nanoparticles (NPs), J. Alloys Compd. 509 (2011) 9399.

[35] V.R. Murthy, J. Sobhananadri, Dielectric properties of some nickel-zinc ferrites at radio frequency, Physica Status Solidi A 36 (1977) K133.

[36] J.C. Maxwell, Electricity and Magnetism, vol. 2, Oxford Universitry Press, New York, 1973.

[37] N. Kumari, V. Kumar, S. Khasa, S.K. Singh, Structural and dielectric investigations on ferrite nanoparticles prepared by chemical co-precipitation method, J. Adv. Phys 3(2) (2014) 111.

[38] N. Singh, A. Agarwal, S. Sanghi, Dielectric relaxation, conductivity behavior and magnetic properties of Mg substituted Zn–Li ferrites, Curr. Appl. Phys. 11 (2011) 783.

[39] K. P. Thummer, H. H. Joshi, R. G. Kulkarni, Electrical and dielectric properties of zincsubstituted magnesium rich manganeseferrites, J. Mater. Sci. Lett. 18 (1999) 1529.

.

[40] M.R. Bhandare, H.V. Jamadar, A.T. Pathan, B.K. Chougule, A.M. Shaikh, The effects of thermal treatment on the physical properties of $Sr_2FeMo_{1-x}M_xO_6$ perovskite with M = W, Ta and $x \leq 0.3$, J. Alloys Compd. 509 (2011) 113.

[41] D.M. Jnaneshwara, D.N. Avadhani, B.D. Prasad, B.M. Nagabhushana, H. Nagabhushana, S.C. Sharma, S.C. Prashantha, C. Shivakumara, Effect of zinc substitution on the nanocobalt ferrite powders for nanoelectronic devices, J. Alloys Compd. 587 (2014) 50.

[42] A.M. Abo El Ata, M. K. El Nirma, S. M. Attia, D. El Kony, A. H. Al-Hammadi, Studies of AC electrical conductivity and initial magnetic permeability of rare-earth-substituted Li–Co ferrites, J. Magn. Magn. Mater. 297 (2006) 33.

[43] H. Bottger, V.V. Bryksin, Hopping Conduction in solids, Akademie-Verlag, Berlin (1985).

[44] R.S. Devan, Y.D. Kolekar, B.K. Chougule, Effect of cobalt substitution on the properties of nickel–copper ferrite, J. Phys: Condens. Matter 18 (2006) 9809.

[45] B. Ramesh, S. Ramesh, R.V. Kumar, M.L. Rao, AC impedance studies on $LiFe_{5-x}Mn_xO_8$ ferrites, J. Alloys Compds. 513 (2013) 289.

[46] N. Kumari, V. Kumar, S.K. Singh, Effect of Cr^{3+} substitution on properties of nano-$ZnFe_2O_4$, J. Alloys. Compds. http://dx.doi.org/10.1016/j.jallcom.2014.10.083

[47] U.N. Trivedi, K.B. Modi, H.H. Joshi, Magnetic Behaviour of the oxide spinels: $Li_{0.5}Fe_{2.5-2x}Al_xCr_xO_4$, Pramana-J. Phys. 58 (2002) 1031.

[48] J. Smith, H.P.J. Wijn, Ferrites, Wiely, New York, 1959.

[49] Wang, Y. Liu, Z. Zang, Handbook of Nanophase and Nanostructured Materials (Vol. III: Materials Systems and Applications I), Kluwer Academic/Plenun Publishers, USA, 2003.

.

[50] E.C. Stoner, E.P. Wohlfarth, A Mechanism of Magnetic Hystersis in Hetrogeneous Alloys, Phil. Trans. R. Soc. Lond. A. 240 (1948) 599.

[51] S. Giri, S. Samanta, S. Maji, S. Ganguli, A. Bhumik, Magnetic properties of α-Fe_2O_3 nanoparticle synthesized by a new hydrothermal method, J. Magn. Magn. Mater. 285 (2005) 296.

[52] N. Kumari, V. Kumar, S. Khasa, S.K. Singh, Chemical synthesis and magnetic investigations on Cr^{3+}substituted Zn-ferrite superparamagnetic nano-particles, Ceram. Int. 41 (2015) 1907.

[53] B.S. Chauhan, R. Kumar, K.M. Jadhav, M. Singh, Magnetic study of substituted Mg–Mn ferrites synthesized by citrate precursor method, J. Magn. Magn. Mater. 283 (2004) 71.

[54] M.J. Iqbal, M.N. Ashiq, P.H. Gomez, J.M.M. Munoj, C.T. Cabrera, Influence of annealing temperature and doping rate on the magnetic properties of Zr–Mn substituted Sr-hexaferrite nanoparticles, J. Alloys Compds. 500 (2010) 113.

.

Table Caption:

Table 1: Crystalline size (D), lattice constant (a), X-ray density (ρ_x), measured density (ρ_m), porosity (P), radii of tetrahedral and octahedral sites r_A and r_B respectively, tetrahedral bond length (d_{AL}), octahedral bond length (d_{BL}), jump length of A-site (L_A) and jump length of B-site (L_B) for $ZnAl_xFe_{2-x}O_4$ (x=0.1, 0.2, 0.3, 0.4 and 0.5) .

Table 2: Relaxation time (τ_g), grain resistance (R_g) and grain capacitance (C_g) for $ZnAl_xFe_{2-x}O_4$ (x=0.1, 0.2, 0.3, 0.4 and 0.5) at 523K.

Table 3: Relaxation time (τ_g), grain resistance (R_g) and grain capacitance (C_g) for $ZnAl_xFe_{2-x}O_4$ (x=0.1) at different temperatures i.e. 423K, 473K, 523K.

Table 4: Particle size (D_T) calculated from TEM micrograph, Particle size (D_M) calculated from hysteresis loop, Saturation magnetization (M_S), Remanance (M_r), coercivity (H_C), anisotropy constant (K), squareness (S) and magnetic moment (η_B).

Figure Captions:

Fig. 1(a) X-ray diffraction pattern of $ZnAl_xFe_{2-x}O_4$ (x=0.1, 0.2, 0.3, 0.4 and 0.5) for all samples calcined at 523K.

Fig. 1(b) Typical EDAX spectrum for $ZnAl_{0.5}Fe_{1.5}O_4$ sample.

Fig. 2 TEM micrograph at different Al^{3+} ion content: (a) x=0.1; (b) x=0.3 (c) x=0.5 calcined at 523K.

.

Fig. 3 Variation of real part of dielectric constant (ε′) of $ZnAl_xFe_{2-x}O_4$ (x=0.1, 0.2, 0.3, 0.4 and 0.5) with frequency at 523K. (Inset: Variation of dielectric constant (ε') with temperature for $ZnAl_xFe_{2-x}O_4$ (x=0.1) at 10kHz, 100kHz, 5MHz.

Fig. 4 Variation of imaginary part of dielectric constant (ε'') of $ZnAl_xFe_{2-x}O_4$ (x=0.1, 0.2, 0.3, 0.4 and 0.5) with frequency at 523K. (Inset: Variation of imaginary part of dielectric constant (ε'') with temperature for $ZnAl_xFe_{2-x}O_4$ (x=0.1) at 1kHz, 100kHz, 5MHz.

Fig. 5 Variation of dielectric loss ($tan\delta$) of $ZnAl_xFe_{2-x}O_4$ (x=0.1, 0.2, 0.3, 0.4 and 0.5) with frequency at 523K. (Inset: Variation of dielectric loss ($tan\delta$) with temperature for $ZnAl_xFe_{2-x}O_4$ (x=0.1) at 10kHz, 100kHz, 5MHz.

Fig. 6 Variation of ac conductivity (σ_{ac}) of $ZnAl_xFe_{2-x}O_4$ (x=0.1, 0.2, 0.3, 0.4 and 0.5) with frequency at 523K. (Inset: Variation of ac conductivity (σ_{ac}) with temperature for $ZnAl_xFe_{2-x}O_4$ (x=0.1) at 10kHz, 100kHz, 5MHz.

Fig. 7(a) Cole-Cole plot for $ZnAl_xFe_{2-x}O_4$ (x=0.1, 0.2, 0.3, 0.4 and 0.5) at 523K**.**

Fig. 7(b) Cole-Cole plot for composition $ZnAl_xFe_{2-x}O_4$ (x=0.1) at different temperatures i.e 423K, 473K, 523K**.**

Fig. 8(a) M-H curve of $ZnAl_xFe_{2-x}O_4$ (x=0.1, 0.2, 0.3, 0.4 and 0.5).

Fig. 8(b) M-H curve of $ZnAl_xFe_{2-x}O_4$ (x= 0.1) in as obtained form and annealed at 523K and 773K.

.

Table 1

X	**0.1**	**0.2**	**0.3**	**0.4**	**0.5**
a**(Å)**	8.396	8.385	8.373	8.346	8.342
D**(nm)**	29.0	28.5	27.8	27.0	25.6
ρ_x**(gm/cc)**	5.343	5.301	5.258	5.243	5.184
ρ_m**(gm/cc)**	1.53	1.47	1.46	1.43	1.39
P	0.683	0.711	0.723	0.725	0.729
r_A**(Å)**	0.4979	0.4954	0.4929	0.4870	0.4862
r_B**(Å)**	0.7792	0.7762	0.7733	0.7661	0.7656
d_{al}**(Å)**	1.8179	1.8154	1.8129	1.8070	1.8062
d_{bl}**(Å)**	2.0992	2.0962	2.0933	2.0866	2.0856
L_A**(Å)**	3.6359	3.6308	3.6258	3.6141	3.6124
L_B**(Å)**	2.9687	2.9645	2.9604	2.9509	2.9495

.

Table 2

X	**0.1**	**0.2**	**0.3**	**0.4**	**0.5**
τ_g **(μsec.)**	2.35	2.56	2.95	73.3	134
R_g **(kΩ)**	108.00	170.45	217.79	6496.38	10826.01
C_g **(pF)**	21.75	15.02	13.50	11.29	12.37

.

Table 3

T(K)	τ_g (μsec)	R_g (kΩ)	C_g (pF)
523	2.35	108.00	21.75
473	7.19	308.72	23.29
423	17.0	711.69	23.88

.

Table 4

Parameter	x=0.1	x=0.2	x=0.3	x=0.4	x=0.5
D_M (nm)	21.6	21.3	21.5	25.3	26.9
M_S	13.29	12.70	12.5	10.11	8.42
M_r	1.128	0.778	0.655	0.385	0.115
H_C (Oe)	88.00	75.27	62.73	53.11	41.35
K (erg/Oe)	1218.26	995.75	812.88	559.31	362.67
S	0.084	0.061	0.052	0.038	0.014
η_B (μB)	0.566	0.535	0.517	0.415	0.341

.

Fig. 1(a)

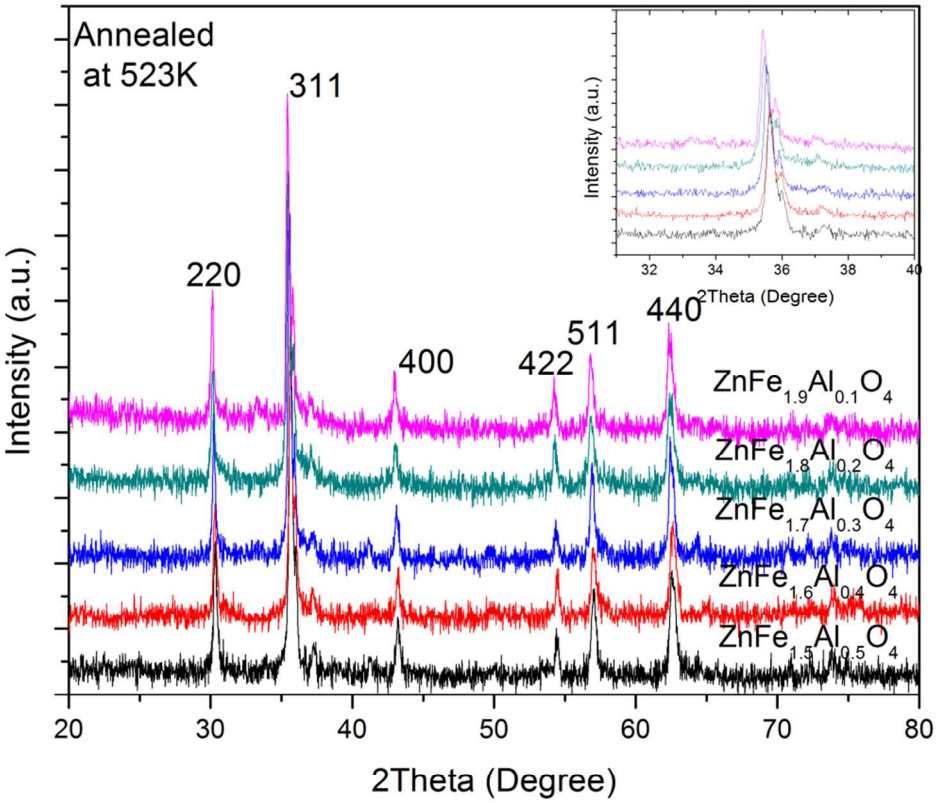

.

Fig. 1(b)

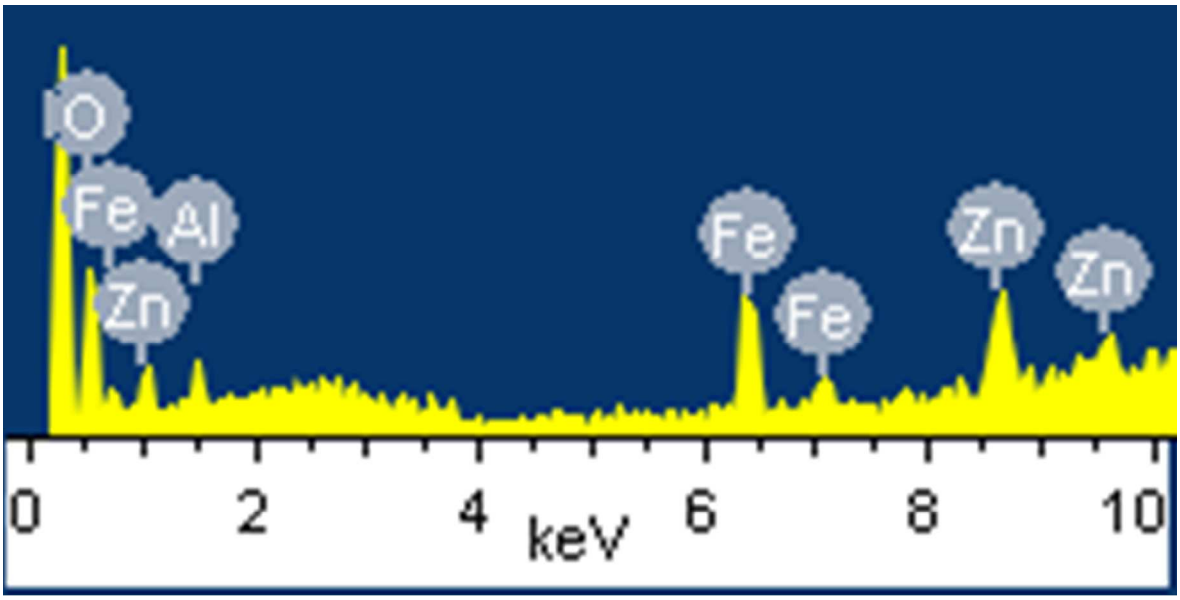

.

Fig. 2(a)

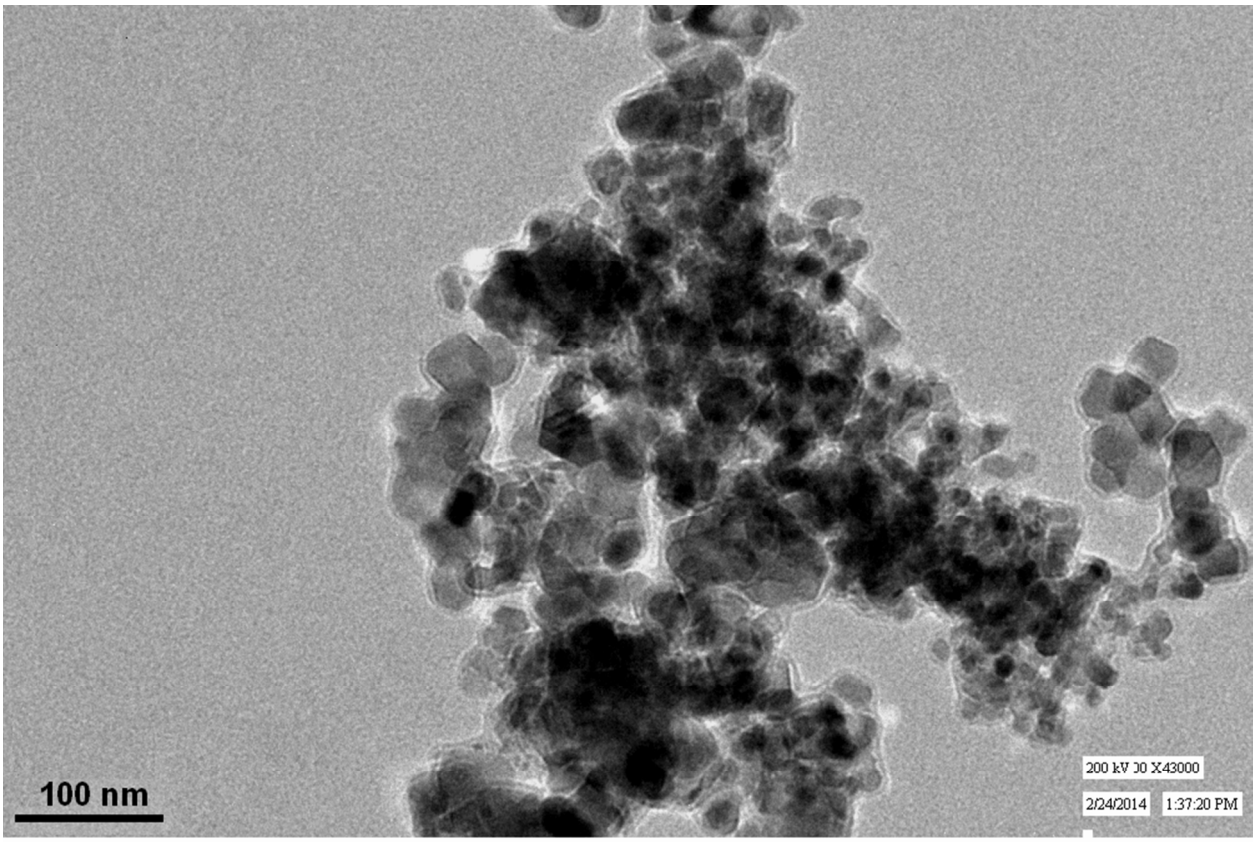

.

Fig 2(b)

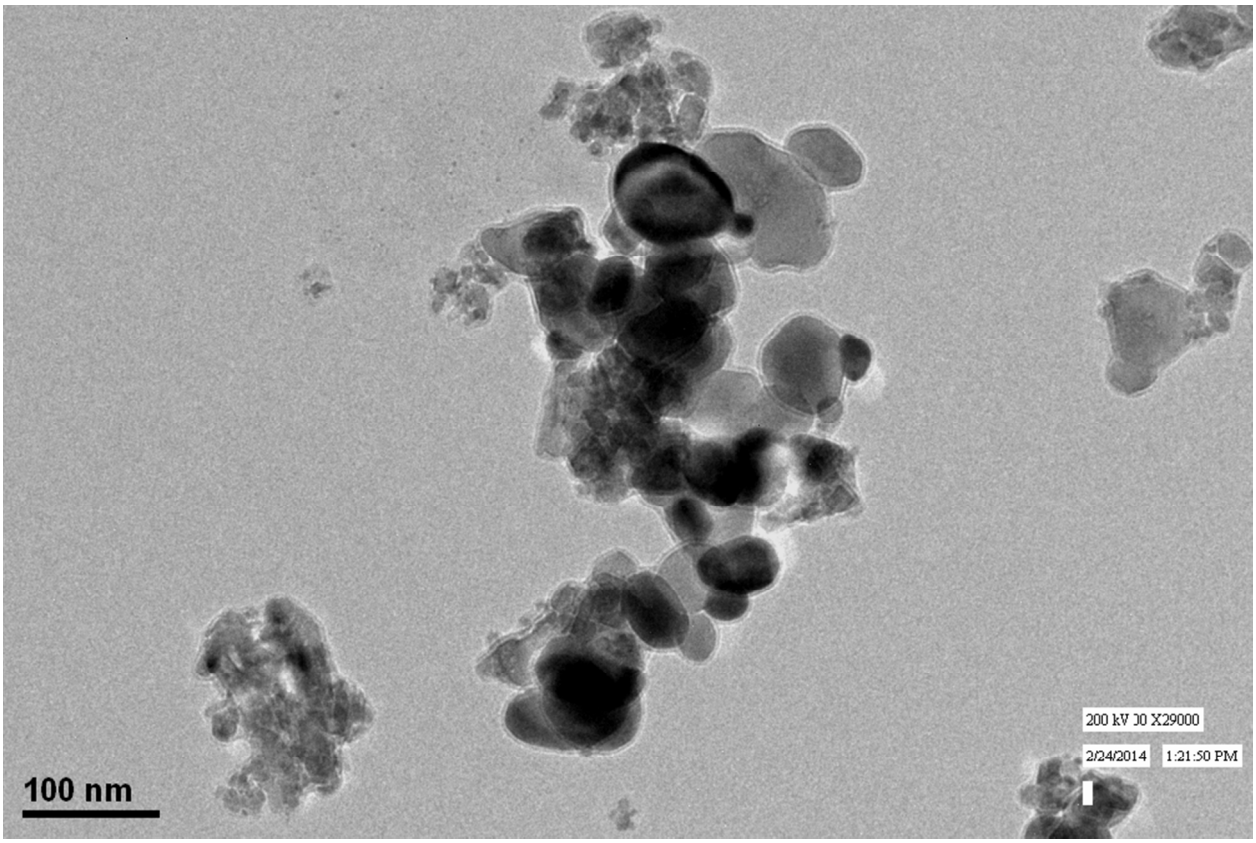

.

Fig 2(c)

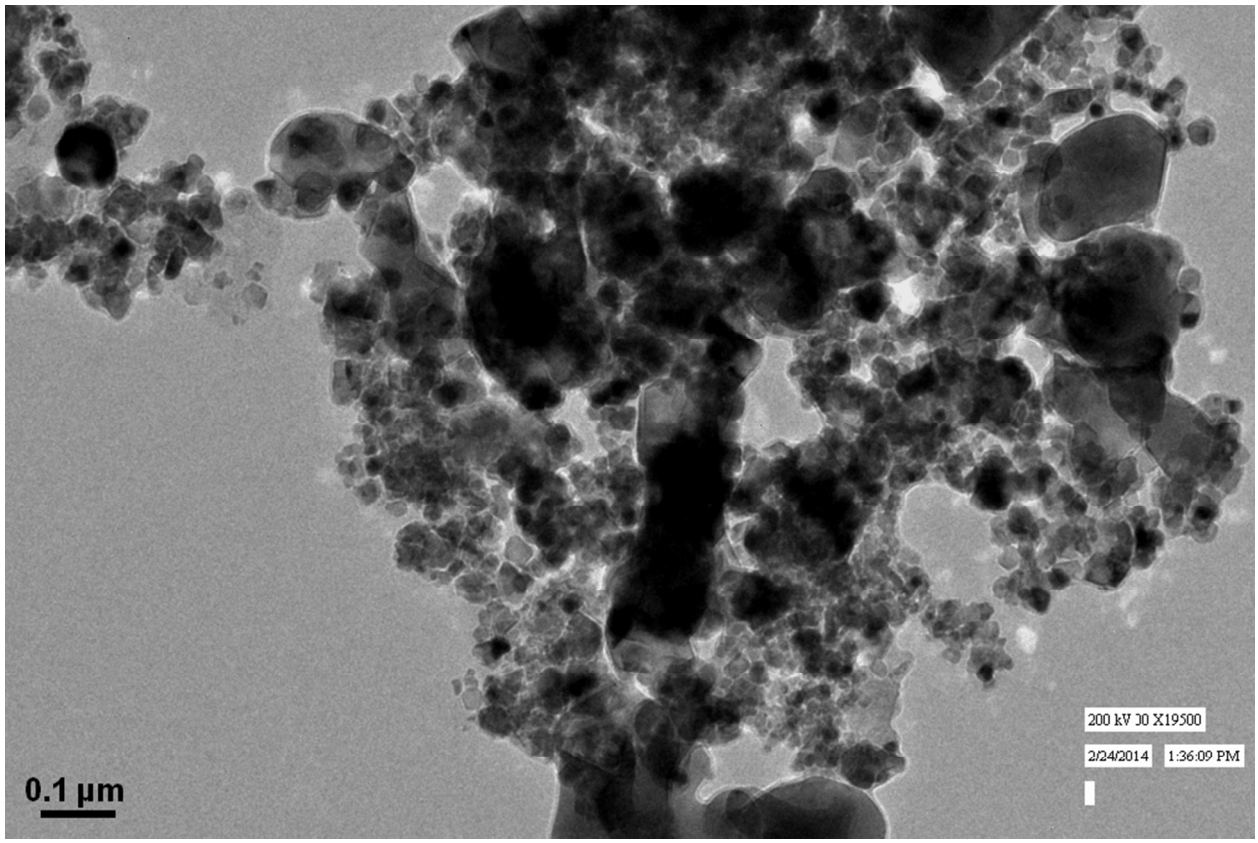

.

Fig. 3

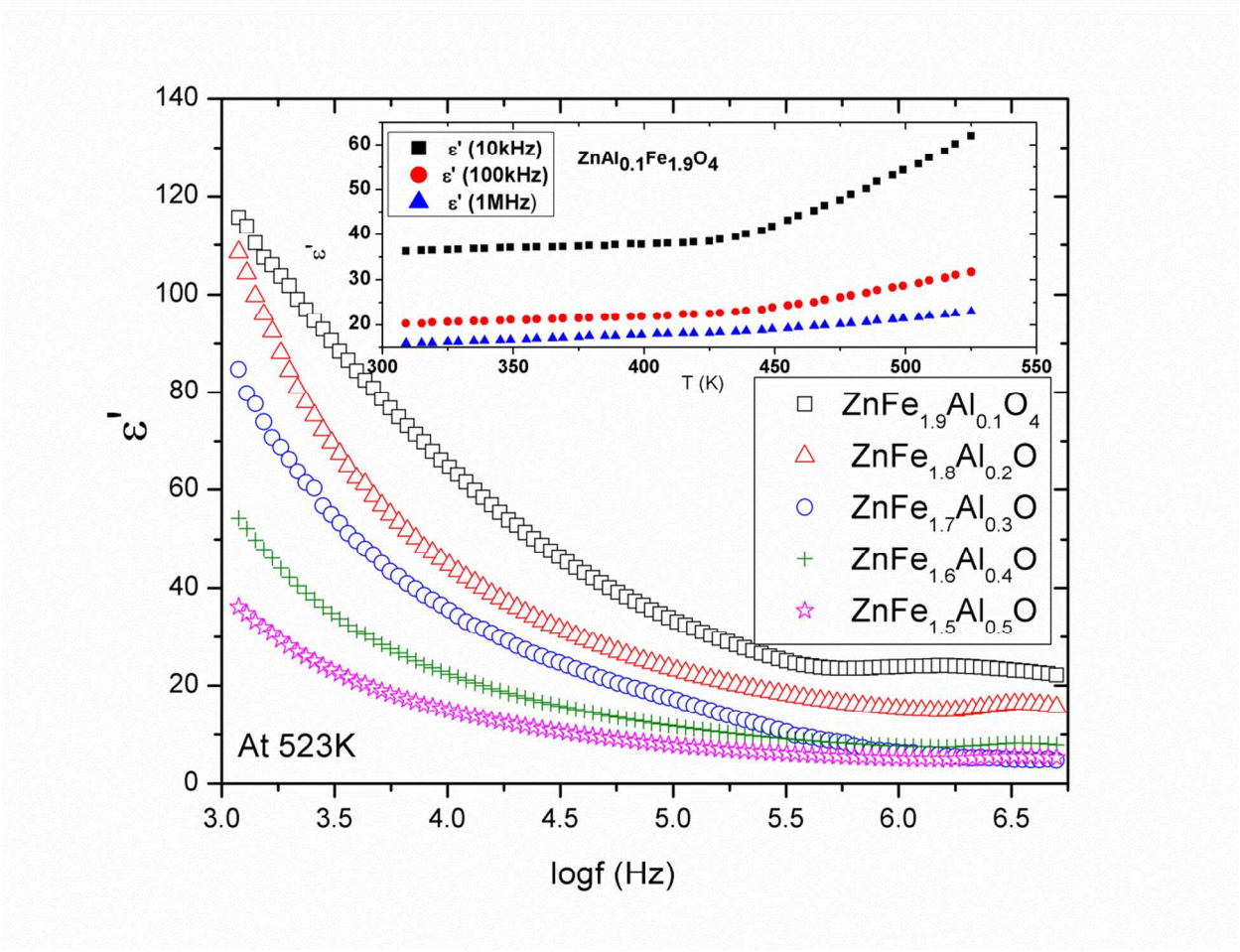

.

Fig. 4

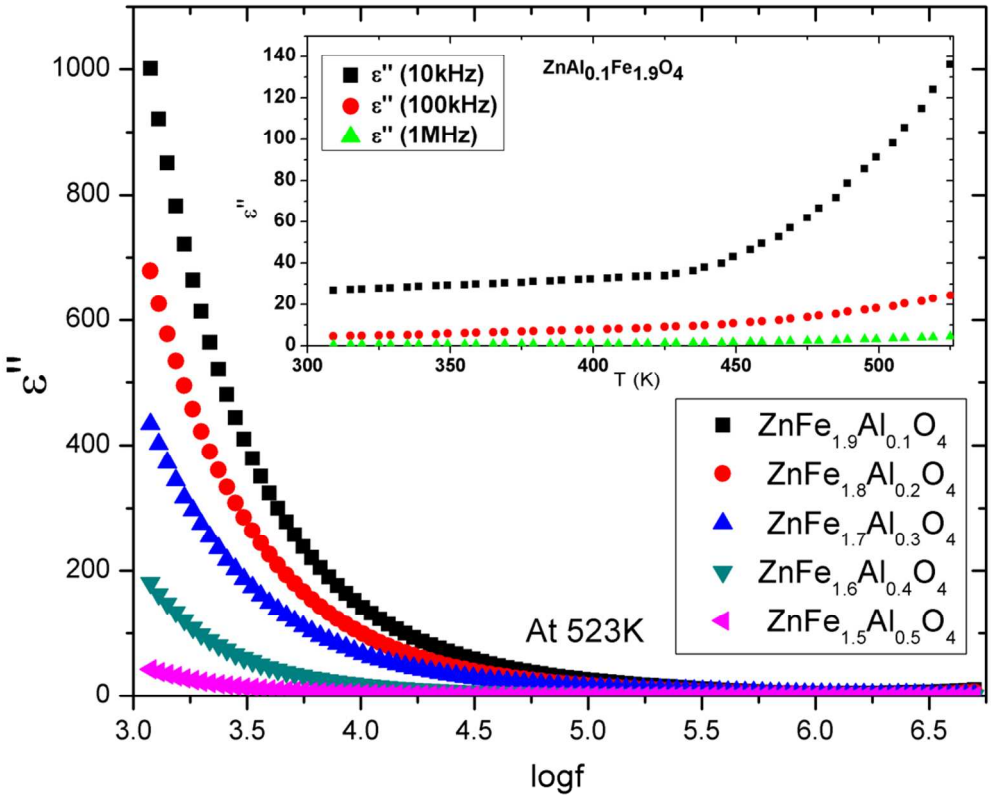

.

Fig. 5

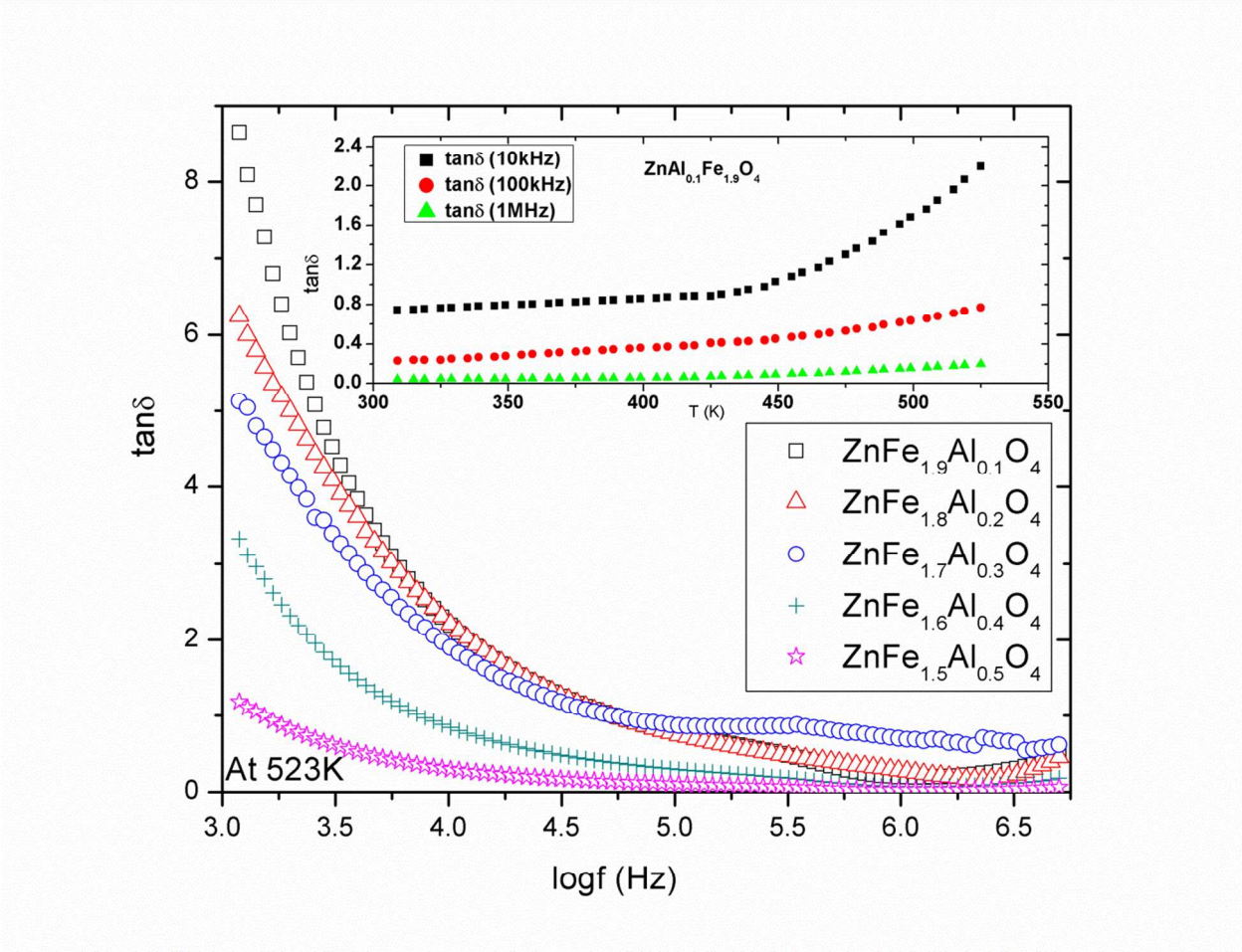

.

Fig. 6

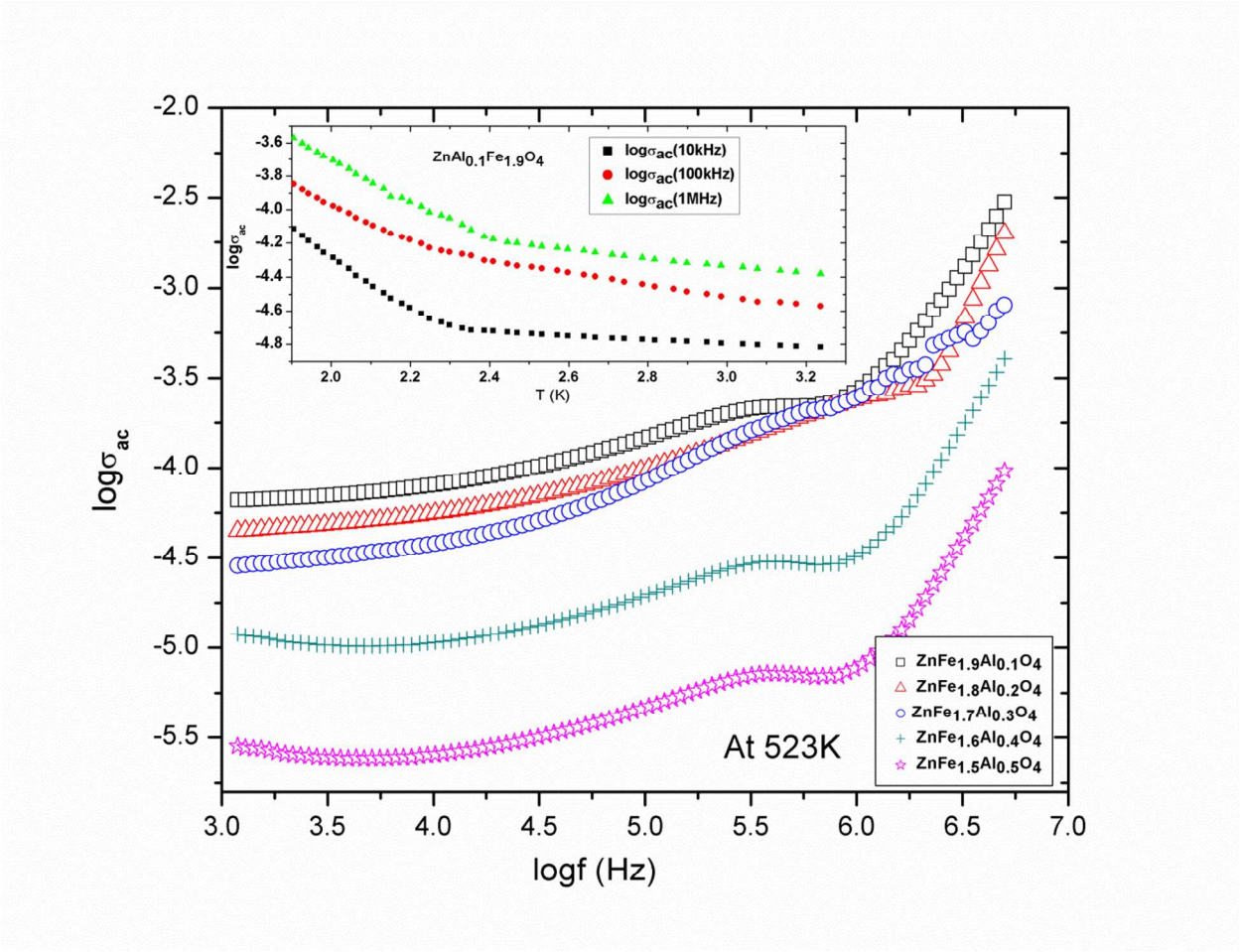

.

Fig. 7(a)

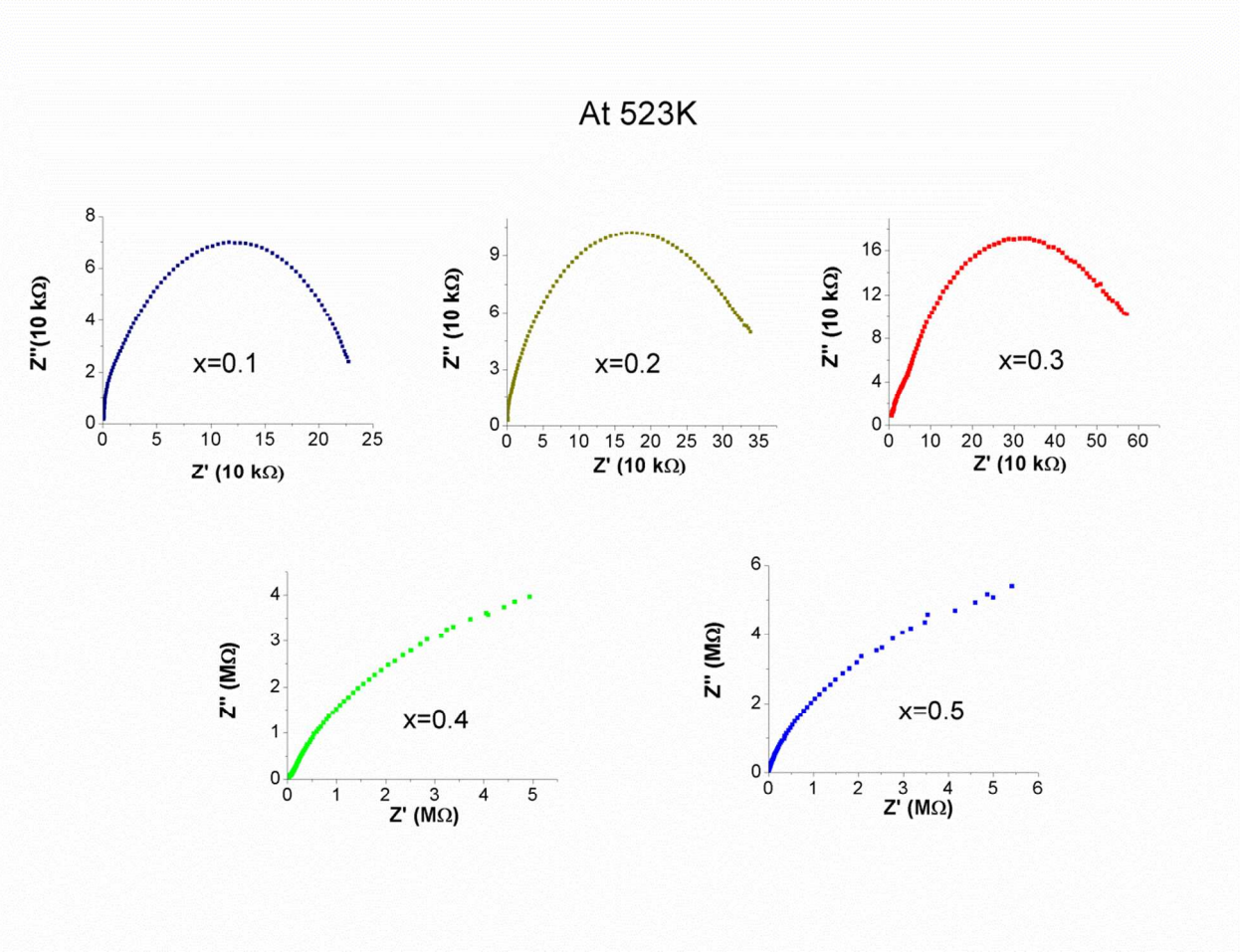

.

Fig. 7(b)

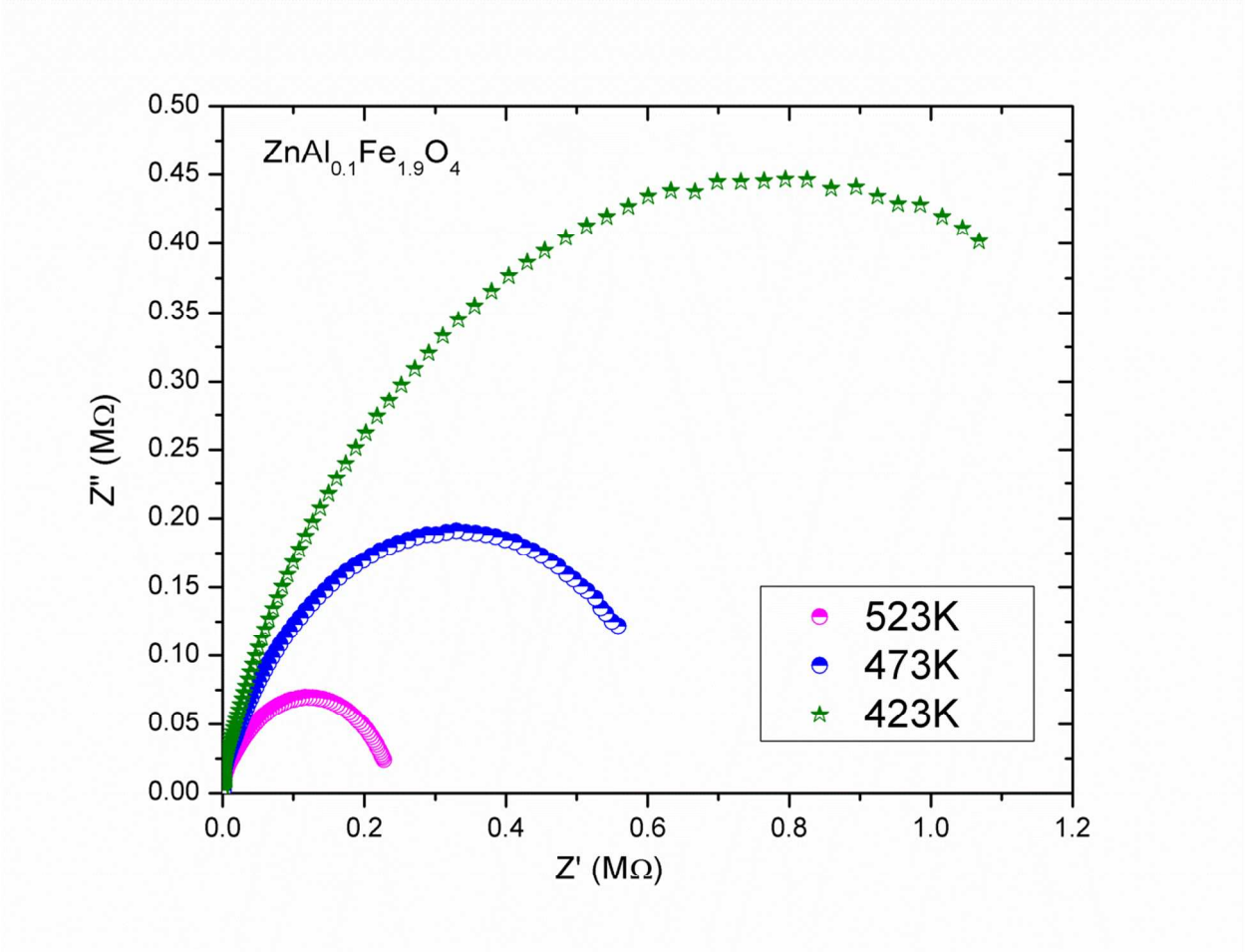

.

Fig. 8(a)

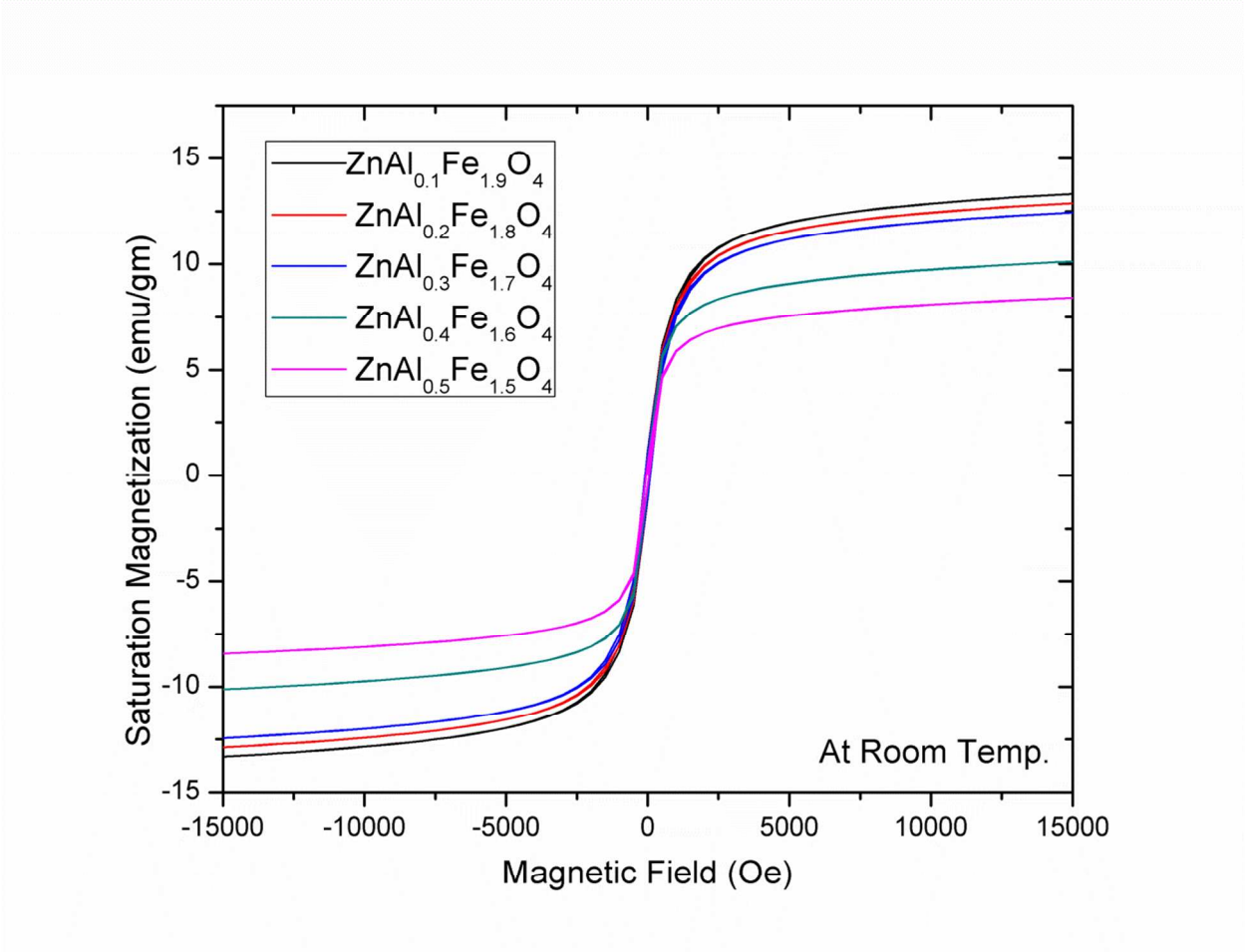

.

Fig. 8(b)